Journal of the Korean Astronomical Society
52: 31 ∼ 40, 2019 April
https://doi.org/10.5303/JKAS.2019.52.2.31
pISSN: 1225-4614 · eISSN: 2288-890X
http://jkas.kas.org

Core-Jet Blending Effects in Active Galactic Nuclei under the Korean VLBI Network View at 43 GHz

Juan-Carlos Algaba[1,2], Jeffrey Hodgson[3], Sin-Cheol Kang[3,4], Dae-Won Kim[2], Jae-Young Kim[5], Jee Won Lee[3], Sang-Sung Lee[3,4], and Sascha Trippe[2]

[1]Department of Physics, Faculty of Science, University of Malaya, 50603 Kuala Lumpur, Malaysia; algaba@um.edu.my
[2]Department of Physics and Astronomy, Seoul National University, Gwanak-gu, Seoul 08826, Korea
[3]Korea Astronomy and Space Science Institute, 776 Daedeokdae-ro, Yuseong-gu, Daejeon 34055, Korea
[4]Korea University of Science and Technology, 217 Gajeong-ro, Yuseong-gu, Daejeon 34113, Korea
[5]Max-Planck-Institut für Radioastronomie, Auf dem Hügel 69, D-53121 Bonn, Germany

Received June 29, 2018; accepted February 24, 2019

Abstract: A long standing problem in the study of Active Galactic Nuclei (AGNs) is that the observed VLBI core is in fact a blending of the actual AGN core (classically defined by the $\tau = 1$ surface) and the upstream regions of the jet or optically thin flows. This blending may cause some biases in the observables of the core, such as its flux density, size or brightness temperature, which may lead to misleading interpretation of the derived quantities and physics. We study the effects of such blending under the view of the Korean VLBI Network (KVN) for a sample of AGNs at 43 GHz by comparing their observed properties with observations obtained using the Very Large Baseline Array (VLBA). Our results suggest that the observed core sizes are a factor ~ 11 larger than these of VLBA, which is similar to the factor expected by considering the different resolutions of the two facilities. We suggest the use of this factor to consider blending effects in KVN measurements. Other parameters, such as flux density or brightness temperature, seem to possess a more complicated dependence.

Key words: galaxies: active — methods: data analysis — techniques: high angular resolution — techniques: interferometric

1. Introduction

The observable morphology of a typical radio-loud active galactic nuclei (AGN) consists of i) the core, an optically thick region classically defined by the $\tau = 1$ surface, and ii) an optically thin jet or emitting region. In general, due to resolution limitations, the observed radio core is actually a blending of the actual AGN core and the upstream regions of the optically thin flows. This becomes very evident when studying the phenomenology of AGNs with instruments achieving further resolution limits: what was first conceived as the core region, can be now seen to contain further structure, consisting of a smaller core and additional emission or jet components.

One of the long-standing problems in the study of these objects is that, even at resolutions of few milliarcseconds, provided by interferometric techniques such as VLBI, this core–jet blending effect can still be significant, as proven by observations by GMVA, VSOP or RadioAstron, which can resolve even further structure from what was considered to be the VLBI core (see, e.g., Boccardi et al. 2016; Asada et al. 2016; Gómez et al. 2016). This blending effect can greatly affect observables, such as polarization, core size, or core shift frequency dependence, as contribution from both the core and the innermost jet regions are integrated together. Thus, such blending has to be treated carefully and an analysis has to be done to properly understand its effects on our observable quantities.

Various methods have been used in the literature to consider such blending effects and its implications in the data analysis. One approach is to consider observations with better resolution and to compare observables, such as the morphology or flux density, to understand how the different resolution may affect these (e.g. Kovalev et al. 2008; Pushkarev et al. 2012). Although better resolutions can be obtained with larger frequency, physical properties of the source may also be different at different frequencies (due to e.g., opacity effects). Thus different arrays or, if possible, different array configurations observing at the same frequencies are preferred for such analysis. A different approach would consist of the convolution of a pre-existing high resolution map with a larger beam size or the flagging of data at various UV-distances in the interferometric UV-plane to simulate a map of lower resolution (e.g. Hovatta et al. 2014). A third approach would include the analysis of Monte Carlo simulations on a predefined model (e.g. Mahmud et al. 2013).

The Korean VLBI Network (KVN) is a unique interferometric array located in the Korean peninsula. Consisting of three 21-m antennas equipped with a multi-receiver band system, it can observe at 22, 43, 86 and 129 GHz, higher frequencies than most other VLBI networks, simultaneously. With baselines between 305–476 km, achievable resolutions at these frequencies can

Corresponding author: J. C. Algaba

reach about $\gtrsim$ 1 mas, which makes the KVN an excellent tool to resolve the innermost regions of AGNs. Nonetheless, as we have mentioned, for a robust analysis, it is necessary to first consider blending effects that can be expected from the KVN view.

A pioneering work where KVN source blending issues are discussed is that of Rioja et al. (2014). Although their work mainly focuses on astrometric issues, they include an analysis of the source structure effects in the KVN, including structure blending effects as compared with both high- and matched-resolution VLBA images. As they find, this blending has a large impact in astrometric measurements, becoming the dominant source of errors in astrometric measurements of extended sources. Its magnitude, however, seems to be different case by case, suggesting that a large sample should be needed for proper study.

In this paper we study properties of the core, such as the core size or core brightness temperature, of several AGNs observed with the KVN and compare them with observations taken with the Very Large Baseline Array (VLBA), an array which offers better angular resolution. In this way, we estimate the core-jet blending and its effects on such observables. Kim et al. (2019) will do parallel analysis using a different approach. This paper is organized as follows: in Section 2 we describe the observations used for our analysis. In Section 3 we show our results and comparison. In Section 4 we discuss these and possible implications. A summary can be found in Section 5.

2. OBSERVATIONS

2.1. Data Selection Criteria

In order to study possible core blending effects, we intend to compare our KVN measurements with other VLBI observations of the same source capable of clearly resolving components or features upstream of the jet that may be blended with the KVN core. Given the strong variability of these objects, with timescales of even just a few days (see e.g. Wagner & Witzel 1995), comparison should ideally be performed with (quasi-)simultaneous observations. For consistency and robustness of the results, one should ideally include various epochs, not too sparse in time, if possible.

However, observations performed (quasi-) simultaneously in different arrays are not always possible, except for very particular cases where the typical VLBI dynamic scheduling is superseded by a strong science case very particular source or event scenarios. An alternative approach to circumvent these limitations is to investigate data obtained for an extended period of time and, if the relative observed variability is not significant, consider the mean values of the observables.

To analyze the KVN data, we used data from the iMOGABA (interferometric monitoring of gamma ray bright AGNs; see Lee et al. 2013; Algaba et al. 2015; Lee et al. 2016) program, which observes a total of 30 well known AGNs with a mean cadence of about a month at 22, 43, 86 and 129 GHz. This is, to date, the best source for AGN monitoring with the KVN array. Unfortunately, there are very few VLBI multi–epoch observations or monitoring programs available for comparison. In particular, the authors are not aware of any VLBI program at 22 or 86 GHz with good cadence. Similarly, the situation at 129 GHz is very unclear since this is not a common VLBI observing frequency. Only at 43 GHz the Boston University VLBA-BU-BLAZAR Program provides an excellent systematic monitoring of AGNs.

Consequently, in this paper we will focus on the comparison of KVN iMOGABA 43 GHz data with the VLBA-BU-BLAZAR program which, thanks to the much larger baselines, provides a resolution better by a factor of $\sim$ 18. Although not complete in terms of frequency space nor in the framework of source characteristics, this will provide a fundamental first step test to understand the KVN core blending effects. With this in mind, we will leave the analysis of other KVN frequencies for a forthcoming study.

One of the first observables that is affected by blending effects is the core size. Indeed, as the observed VLBI core is a combination of the $\tau = 1$ surface (the actual core) and the innermost unresolved regions of the jet, blending plays a significant role in its resulting observed size. The larger the innermost jet regions merged with the core due to blending, the larger the apparent observed size of the core will be. Being one of the direct quantities that can be easily measured in VLBI observations, the core size seems like an ideal proxy to consider the blending effects. Similarly, flux density is a very straightforward observable that can also be affected by the area measured. Finally, the brightness temperature combines these two factors and has proven to be a quantity of great importance in high resolution mapping (see e.g., Bruni et al. 2017; Kardashev et al. 2017; Pilipenko et al. 2018). Thus, in this work, we will consider these three different observables.

2.2. The Data

Information of the data obtained from the VLBA-BU-BLAZAR program, including model-fitting and properties of the VLBA core flux density and size is summarized in Jorstad et al. (2017). We note however that, although this program is still ongoing, Jorstad et al. (2017) limit their analysis to epochs prior to June 2013. In some cases, we were able to access the later public data and continue the model–fit of the source for subsequent epochs (such as for e.g., 1633+382; see Algaba et al. 2018a,b, for further details). The VLBA-BU-BLAZAR program does not contain information about M87. For this source, we used VLBA data from Hada et al. (2013), which contains a total of 7 epochs observations at 43 GHz, once upper limits of the core size are excluded from the analysis. VLBI core flux densities are not shown in this paper, but we used a fiducial value of 0.7 Jy (Ly et al. 2007; Walker et al. 2018).

Regarding the KVN data from the iMOGABA program, only a handful of iMOGABA sources have currently been analyzed in depth. Other sources are

still being investigated or under analysis. Data for 0716+714 is publicly available in Lee et al. (2017); data for 1156+295 is described in Kang et al. (2019); data for 1633+382 is summarized in Algaba et al. (2018a,b); data from M87 can be inspected in Kim et al. (2018); and data for BL Lac is investigated in Kim et al. (2017). In order to obtain state-of-the-art information regarding the properties of the rest of the sources, an iMOGABA modelf-fitting DIFMAP script has been implemented (Hodgson et al. 2016). In a nutshell, this script finds the best model based on a circular Gaussian fit to the core. This is expected to work well given that iMOGABA sources at 43 GHz are mostly either point-like or core-dominated. KVN uncertainties at 43 GHz should be close to 10%. A detailed discussion is provided in Lee et al. (2016).

In Figure 1 we show the results obtained with this script compared with the more robust manual analysis which may include, in some cases, additional components. It is clear that, considering their uncertainties, the flux densities obtained with the script are quite reliable and closely follows those obtained with a more careful analysis. The core sizes seem to also roughly match, except for the cases of extended structures with significant flux, such as that of 0716+714 or BL Lac, where the script overestimates the size. Nonetheless, such difference is a factor of $\lesssim 2$ at most, which is not dramatic for our study and, as mentioned earlier, will happen in only very few cases. We thus consider that, in a statistical sense, the script works well for our purposes here.

3. RESULTS

Flux densities and core sizes were obtained for 25 sources. Brightness temperatures were calculated using the relationship $T_b = 1.22 \times 10^{12} S(1+z)/43^2/d^2$, where S and d are the model fitted core flux densities and core sizes. Compiled data can be examined in Figure 2. In general, we were not able to obtain (quasi-) simultaneous data, and there is a gap between VLBI and KVN data for most of the sources, except for the case of 1633+382 and 1156+295. It seems however that, whilst certain variability, inherent to these sources, is still clear, its dispersion in terms of the quantities observed here is not too critical for our purposes. In fact, it seems that the dispersion is of the same order as the respective measured quantities, if not smaller. On the other hand, comparison between the KVN and VLBI arrays show that, whereas the measured flux densities appears to be quite similar for many sources, measured core sizes and brightness temperatures are different in the two arrays by at least an order of magnitude. Table 1 summarizes the median values of flux density and core size calculated among all sources and their dispersion in a quantitative manner.

In Table 2 we summarize some relevant source properties and the average quantities obtained from our data. Columns 1, 2 and 3 show the source name, its redshift and it viewing angle, from Hovatta et al. (2009). Columns 4, 5 and 6 indicate the core flux S under the VLBA and KVN perspectives, and a compactness factor, $f_S = S^{VLBA}/S^{KVN}$. Columns 7, 8 and 9 show the core size d under the VLBA and KVN perspectives, and the core size ratio $f_d = d^{VLBA}/d^{KVN}$. Similarly, columns 10, 11 and 12 show the core brightness temperature T_b under the VLBA and KVN perspectives, and the core brightness temperature ratio $f_{T_b} = T_b^{VLBA}/T_b^{KVN}$. Statistical values for the fractional quantities are shown in Table 4, and a histogram is shown in Figure 3.

Table 1
Sample Median Quantities

Array	Flux (Jy)	Size (mas)	T_b (K)
VLBA	1.2 ± 0.7	0.06 ± 0.02	$(2.5 \pm 2.6) \times 10^{11}$
KVN	2.1 ± 1.3	0.77 ± 0.27	$(4.1 \pm 4.5) \times 10^{9}$

3.1. Notes on Individual Sources

Below, we indicate some remarks for a number of sources for which the assumptions stated above (small variability, etc) may not apply. In effect, these sources may provide some bias for the discussion, and care should be taken when considering their observed quantities and derived fractional values.

– *3C84:* Significant amount of upper limits were found for the core size in this source, suggesting that the actual core is much smaller than what the KVN can resolve at 43 GHz. As a consequence, no brightness temperatures were calculated for such upper limits.

– *0420-014:* The compactness factor is $f_S > 1$ for this source. However, the observed flux with VLBA seems to connect well with the one with KVN. We suggest that this larger value may be rather caused by variability effects.

– *0528+134:* The observed VLBA flux of this source appears to be larger than its KVN flux. Given that the resolution of KVN is smaller and, a priori, the core flux should include a larger region, possibly leading to larger flux densities, if any, we consider the large compactness factor $f_S > 1$ for this source to be also due to variability effects.

– *OJ287:* The flux density of this source seems to be steadily increasing. As a consequence, even when the VLBA flux smoothly connects with the KVN flux, suggesting a ratio close to unity, the actual VLBA and KVN median values appear to be different, leading to a fiducial compactness=0.4

– *1222+216:* The flux density seems to be significantly varying in this source, with two clear maxima in the data. There is a local minimum located in the VLBA data, which may bias the compactness of this source to a value lower than the one which would be expected.

– *3C454.3:* Significant flux variability is found in this source for the VLBA data, with several minima found. The data for KVN suggests a more stable flux density after a small increase.

Table 2
Sources Median Quantities

Source (1)	z (2)	$\theta(^\circ)$ (3)	S^{VLBA}(Jy) (4)	S^{KVN}(Jy) (5)	f_S (6)	d^{VLBA}(mas) (7)	d^{KVN}(mas) (8)	f_d (9)	$T_b^{VLBA}(\times 10^{10}$K) (10)	$T_b^{KVN}(\times 10^{10}$K) (11)	f_{T_b} (12)
0235+164	0.940	0.4	1.08 ± 0.95	1.31 ± 0.51	0.8	0.05 ± 0.02	0.60 ± 0.26	0.09	32.00 ± 38.66	0.39 ± 0.45	81.5
3C84	0.018	39.1	2.69 ± 0.92	6.74 ± 4.01	0.4	0.12 ± 0.03	1.88 ± 1.95	0.06	12.60 ± 11.77	0.38 ± 0.72	33.5
3C111	0.048	15.5	0.83 ± 1.17	1.27 ± 1.22	0.7	0.06 ± 0.04	0.70 ± 0.23	0.09	18.40 ± 19.34	0.17 ± 0.54	106.8
0420-014	0.915	1.9	2.32 ± 1.03	1.50 ± 1.38	1.6	0.07 ± 0.03	0.64 ± 0.26	0.11	32.70 ± 26.04	0.48 ± 0.75	68.2
0528+134	2.060	1.6	1.56 ± 1.28	0.94 ± 0.20	1.7	0.04 ± 0.02	0.66 ± 0.20	0.06	54.65 ± 87.93	0.45 ± 0.31	121.2
0716+714	0.127	5.2	1.72 ± 0.91	2.01 ± 0.72	0.9	0.04 ± 0.01	0.27 ± 0.14	0.14	74.36 ± 103.08	1.57 ± 1.91	47.2
0735+178	0.424	...	0.25 ± 0.09	0.64 ± 0.16	0.4	0.10 ± 0.03	0.80 ± 0.29	0.13	1.77 ± 1.08	0.08 ± 0.13	21.5
0827+243	0.939	3.9	0.76 ± 0.71	0.63 ± 0.36	1.2	0.06 ± 0.03	0.64 ± 0.32	0.09	15.80 ± 39.09	0.21 ± 0.44	74.0
0836+710	2.170	3.2	1.40 ± 0.73	1.36 ± 0.45	1.0	0.07 ± 0.02	1.11 ± 1.29	0.06	19.15 ± 15.77	0.23 ± 0.34	84.8
OJ287	0.306	3.3	1.68 ± 0.60	4.13 ± 1.87	0.4	0.04 ± 0.01	0.51 ± 0.45	0.07	90.95 ± 85.76	1.57 ± 1.42	57.8
1055+018	0.890	4.7	2.40 ± 0.57	2.22 ± 0.71	1.1	0.05 ± 0.01	0.36 ± 0.07	0.13	84.75 ± 65.23	2.39 ± 0.26	35.4
Mrk421	0.030	...	0.22 ± 0.05	0.32 ± 0.42	0.7	0.07 ± 0.03	0.65 ± 0.82	0.11	3.15 ± 2.65	0.05 ± 0.06	61.1
1156+295	0.729	2.0	0.96 ± 0.63	1.15 ± 0.64	0.8	0.04 ± 0.02	0.54 ± 0.24	0.08	55.11 ± 77.20	0.61 ± 1.68	90.0
1222+216	0.435	5.1	0.77 ± 0.45	1.48 ± 0.48	0.5	0.04 ± 0.02	1.20 ± 0.19	0.03	46.90 ± 37.55	0.10 ± 0.06	453.1
3C273B	0.158	3.3	3.14 ± 2.27	8.58 ± 4.19	0.4	0.08 ± 0.04	1.01 ± 0.42	0.08	33.15 ± 77.33	0.74 ± 1.01	44.7
M87	0.004	14.0	0.70 ± 0.00	1.40 ± 0.15	0.5	0.11 ± 0.01	0.54 ± 0.11	0.20	3.83 ± 0.86	0.31 ± 0.15	12.5
1308+326	0.996	3.2	1.04 ± 0.66	1.01 ± 0.37	1.0	0.07 ± 0.02	0.70 ± 0.27	0.10	15.80 ± 10.28	0.21 ± 0.31	74.4
1510-089	0.361	3.4	1.63 ± 0.78	2.57 ± 1.41	0.6	0.06 ± 0.04	0.89 ± 0.54	0.07	30.50 ± 55.44	0.35 ± 0.66	87.2
1633+382	1.813	2.5	2.10 ± 0.75	3.41 ± 1.65	0.6	0.05 ± 0.03	0.44 ± 0.27	0.11	158.65 ± 276.18	3.82 ± 7.10	41.5
3C345	0.595	5.1	1.40 ± 0.39	3.46 ± 0.94	0.4	0.05 ± 0.01	0.50 ± 0.23	0.10	45.15 ± 43.99	1.34 ± 1.05	33.7
NRAO530	0.902	3.0	1.90 ± 0.82	3.17 ± 0.69	0.6	0.05 ± 0.02	1.02 ± 0.30	0.05	50.10 ± 59.91	0.41 ± 0.21	121.0
1749+096	0.322	3.8	2.50 ± 0.93	2.69 ± 0.79	0.9	0.04 ± 0.01	0.63 ± 0.24	0.06	124.00 ± 91.75	0.69 ± 0.46	179.4
BL Lac	0.069	7.3	1.84 ± 0.74	2.48 ± 2.21	0.7	0.03 ± 0.02	0.37 ± 0.20	0.09	126.30 ± 390.97	2.02 ± 4.01	62.5
CTA102	1.037	3.7	1.31 ± 0.90	2.35 ± 1.04	0.6	0.06 ± 0.03	0.60 ± 0.20	0.10	30.25 ± 51.59	0.92 ± 0.73	32.9
3C454.3	0.859	1.3	8.87 ± 6.51	14.40 ± 4.88	0.6	0.06 ± 0.02	0.59 ± 0.20	0.09	184.50 ± 334.00	5.36 ± 3.87	34.4

Table 3
Selected Sources Quasi-Simultaneous Median Quantities

Source (1)	z (2)	$\theta(^\circ)$ (3)	S^{VLBA}(Jy) (4)	S^{KVN}(Jy) (5)	f_S (6)	d^{VLBA}(mas) (7)	d^{KVN}(mas) (8)	f_d (9)	$T_b^{VLBA}(\times 10^{10}$K) (10)	$T_b^{KVN}(\times 10^{10}$K) (11)	f_{T_b} (12)
0716+714	0.127	5.2	1.72 ± 0.91	2.01 ± 0.72	0.9	0.04 ± 0.02	0.30 ± 0.14	0.11	90 ± 103.08	1.30 ± 1.91	68.2
1156+295	0.729	2.0	0.96 ± 0.63	1.15 ± 0.64	0.8	0.04 ± 0.02	0.49 ± 0.26	0.08	330 ± 77.20	0.48 ± 1.68	136.0
1633+382	1.813	2.5	2.10 ± 0.75	3.41 ± 1.65	0.7	0.05 ± 0.01	0.44 ± 0.27	0.09	660 ± 276.18	3.82 ± 7.10	86.5

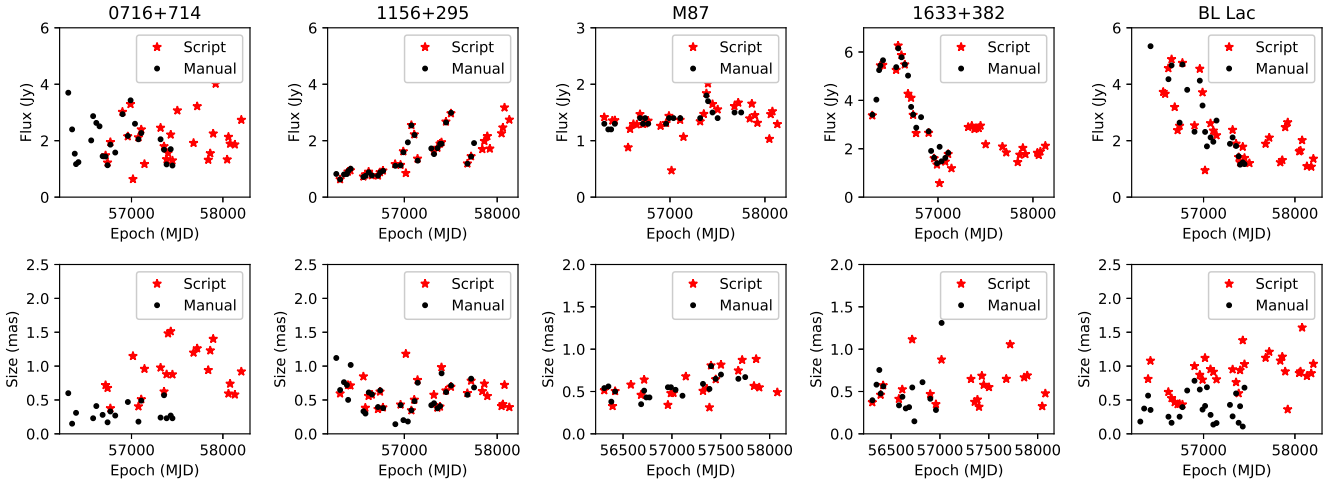

Figure 1. Comparison of the flux densities (top) and core sizes (bottom) obtained using the iMOGABA model fitting script (red stars) and manual fitting (black dots).

Table 4
Sample Fractional Quantities

	f_S	f_d	f_{T_b}
Minimum	0.4	0.03	12.5
25% Quartile	0.5	0.07	36.9
50% Quartile	0.6	0.09	61.8
75% Quartile	0.9	0.11	86.6
Maximum	1.6	0.20	453.1

4. DISCUSSION

As expected, due to the comparatively poorer resolution of the KVN, both the observed flux densities and core sizes appear to be larger than those from the VLBA. In the case of the flux densities, the factor f_S provides information about the compactness of the source. Given an extended structure, integration of the flux over a larger region will result in a larger value, but not all of such flux will actually arise from the more unresolved region observed within the larger array. In our case, $f_S \sim 0.6$ suggests that, on average, VLBA can observe roughly only 60% of the KVN flux or, inversely, 40% of the flux considered to be arising from the VLBI KVN core may be emitted in other regions (although a proper study using convolved images should confirm this; see Kim et al. 2019). Note however that this value changes dramatically with different sources, as shown by the various quartiles. In some sources (e.g., 3C84, 0735+178, OJ287, 3C273B, 3C345), more than half of the core KVN flux can be attributed to blending effects, whereas in more compact ones (e.g., 0716+714, 0836+710, 1308+326) most of the KVN flux seems to arise from the core regions. This is in agreement with the discussion in Rioja et al. (2014), where they suggest that the magnitude of the blending strongly depends on the source.

Maximum baselines for the case of VLBA are of the order of 8611 km (between Mauna-Kea and Saint-Croix antennas), leading to resolutions of the order of 0.17 mas at 43 GHz. On the other hand, maximum KVN baselines are of the order of 476 km (between Tamna and Yonsei antennas), leading to resolution of about 3.0 mas. This is an improvement of the resolution by a factor of 18 when using the VLBA array for 43 GHz. We note however that the maximum baselines (and hence, the smaller beam sizes) will only occur in ideal cases, and the actual baselines will be determined by several other factors such as source elevation. In order to investigate this in detail, we have performed a check as follows: we obtained typical beam sizes from VLBA data (Jorstad et al. 2017) and iMOGABA data (Lee et al. 2016) and obtained the fraction f_{beam}=beam(VLBA)/beam(KVN) on a source-by-source basis. Once we consider the more realistic beam sizes, rather than the maximum baselines, the factor in resolution between VLBA and KVN become $f_d \sim 1/10$, which is much closer to the 50% quartile for f_d. We thus consider that, although they may have a slightly effect, the baseline length is not significantly affecting our results.

There is however no significant correlation found between f_{beam} and f_S (Pearson $r = 0.07$), and only moderate for f_{beam} and f_d ($r = 0.47$). Additionally, the normalized standard deviation $\sigma(f_{beam}/f_{beam}^{max}) = 0.07$ is much smaller than the normalized standard deviation for f_S and f_d (0.23, 0.21, respectively). We have checked that the beam size for the BU-VLBA observations can change by a factor of $\lesssim 11\%$. Similarly, the beam size of the beam size for iMOGABA observations change by a factor $\lesssim 10\%$. This is smaller than the dispersion that we find in the factors f_S and f_d, which can vary by about an order of magnitude. This suggests that the dispersion found in the values for f_S and f_d may have a different origin.

The derived value for the brightness temperature also get severely affected as a consequence of the two factors f_S and f_d. In principle, as we use a larger array,

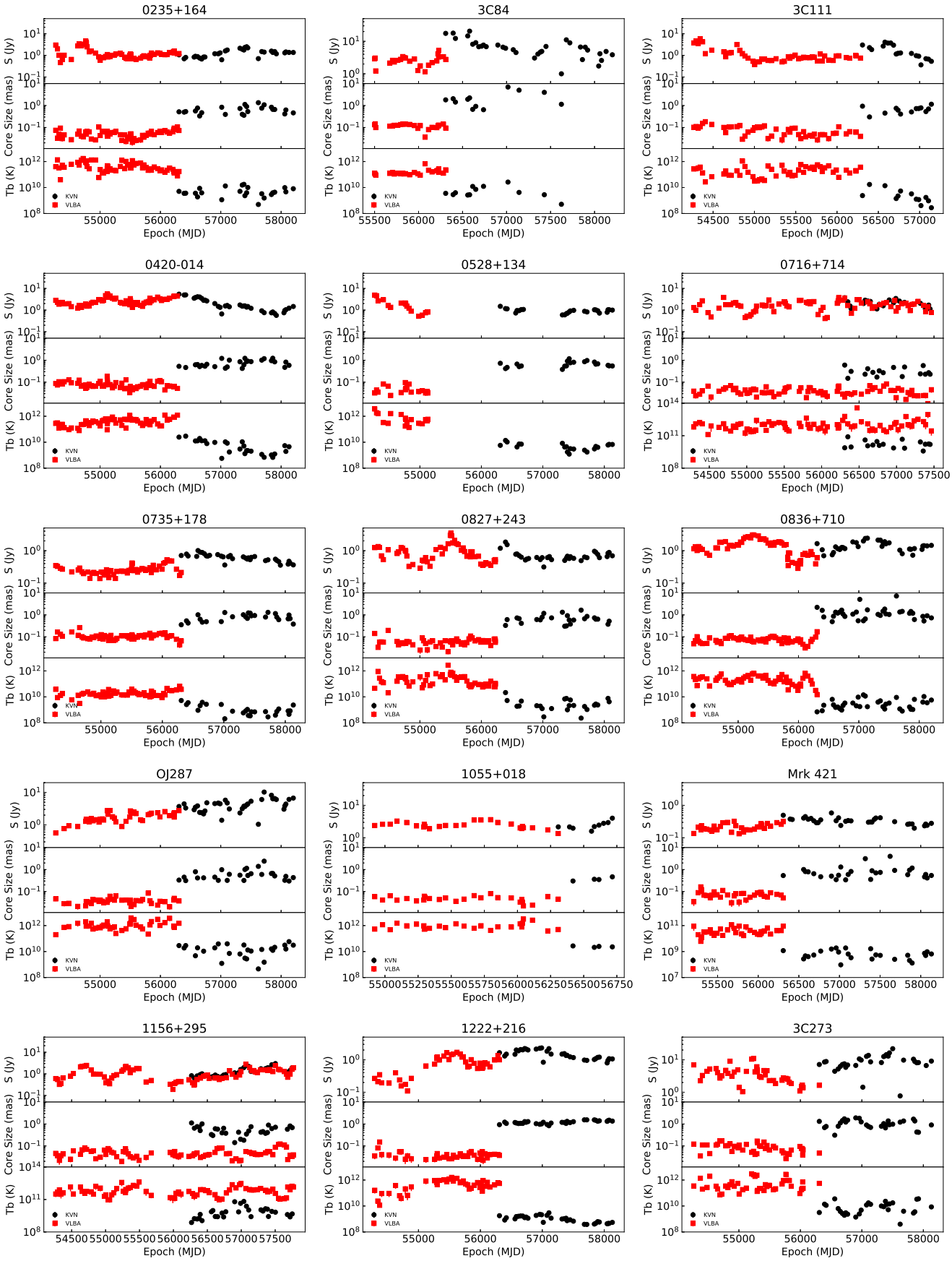

Figure 2. Comparison of core sizes and brightness temperatures observed with VLBA (red squares) and KVN (black circles).

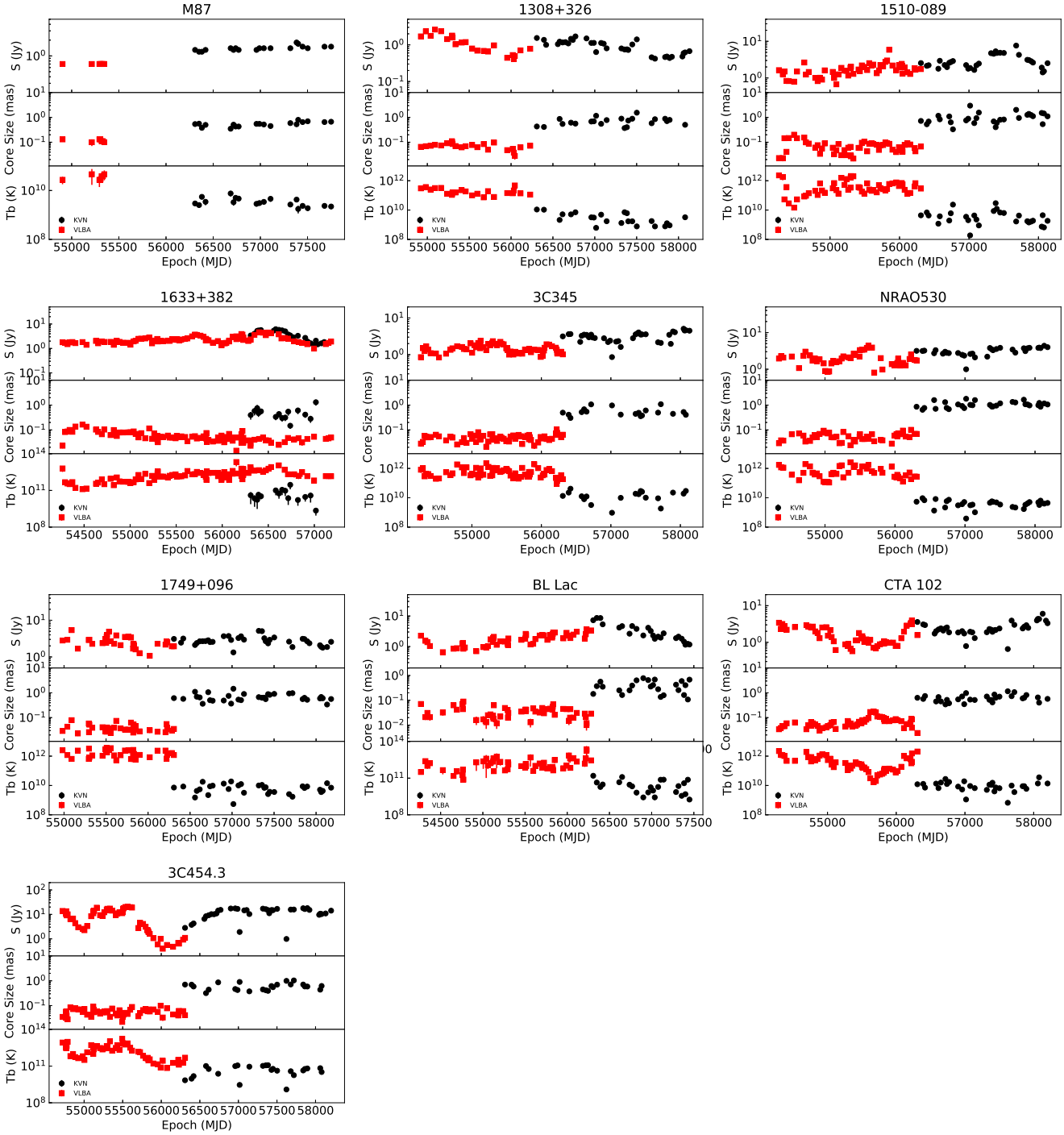

Figure 2. *Continued.*

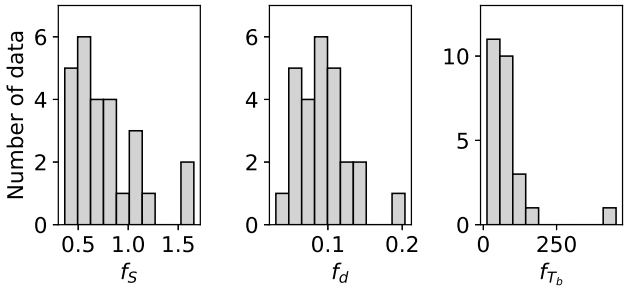

Figure 3. Histograms for the measured fractional quantities f_S, f_d and f_{T_b}.

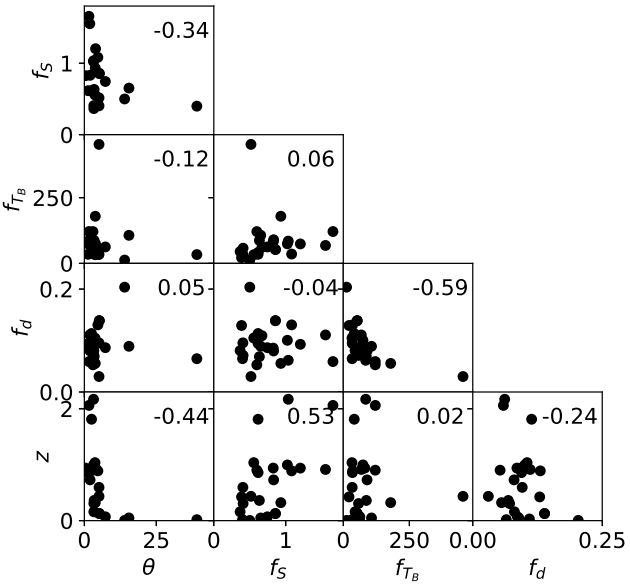

Figure 4. Scatter matrix for the proposed correlations. The correlation coefficients are shown in the top right corner of each panel.

we should be able to probe smaller regions. At the same time, if the source were uniform, we would also observe smaller flux densities in the proportion $S \propto d^2$, thus leading to a similar T_b. However, this is clearly not the case in AGNs in general, with a brighter core and blending effects. In our case here, on average VLBA fluxes are 60% smaller but sizes values become only 9% of their KVN value. This large disproportion results in brightness temperatures $10^{1-2.5}$ times larger with the VLBA array.

4.1. Origin of the Dispersion in f_S and f_d

The dispersion that we find in the fractional values seems to be quite significant and cannot be attributed only to the measurement uncertainties. Identifying the origin of such large dispersion is crucial to assess a proper factor in accounting for core properties with the KVN. It is possible that the source itself plays an important role due to blending effects.

The derived parameters for each source may be intrinsically different due to i) compactness (an increase of the resolution would not significantly affect the observables of a compact source), ii) small viewing angles (leading to components appearing closer in projection), or iii) different redshift (features would appear smaller). Based on this, we consider any possible dependence on the size and brightness temperature factors f_d and f_{T_b} in terms of the compactness f_S, redshift z and viewing angle θ of the sources. In Figure 4 we show the proposed correlations, including the Pearson correlation coefficient r. Inspection of the figure clearly shows that there seems to be no relevant dependence of the blending with compactness, redshift or viewing angle.[1]

Alternatively, since blazars are highly variable in structure and in flux, the blending effect is highly time-dependent. Such variability may produce changes, or even spurious values, in the measured fractional parameters f_S and f_d if comparison is not made properly. Since, the two data sets, KVN and VLBA, used here are not fully coincident in time, variability effects may play a major role. Indeed, although we considered observations over a long period of time to circumvent the need for quasi-simultaneous observations, we found that for all sources, the flux density standard deviation was larger than 15% the median flux, suggesting a significant variability. Indeed, we note that i) the most extreme value $f_d = 0.03$ corresponds to 1222+216, which has been noted to have an observational bias and ii) the sources containing quasi-simultaneous VLBA and KVN data (0716+714, 1156+295, and 1633+382) seem to have similar f_d values. Thus, data analysis of non-overlapping time may have introduced uncertainties and probably biases.

Reflecting this, we consider the sources above mentioned, 0716+714, 1156+295 and 1633+382, and focus on the epochs which have KVN and VLBA data overlapped in time. In Table 3 we summarize the new quasi-simultaneous median quantities for these sources. It seems that the values of f_d for these sources, which were already close, become more similar when not only all the data range but only quasi-simultaneous data is considered. As a different check, we also considered the effect of removing the quasi-simultaneous data for these sources and performed various tests flagging VLBA data near in time to that of the KVN (for example, flagging VLBA data after MJD$>$ 56000, as a simple case). We found that the values for f_d significantly changed, with cases where $f_d = 0.19$ for 1633+382, or $f_d = 0.14$ for 0716+714. This suggests that variability effects are indeed the source for the dispersion in the f_d values. We thus suggest a blending factor for the KVN of $f_d \sim 0.09$.

It seems, on the other hand, that f_S is intrinsically source-dependent, and there doesn't seem to be a simple recipe to determine this parameter. Not only the compactness of the source but a full analysis of its

[1] Note that some fiducial correlation appears due to observational bias (θ vs z) or parameters dependence (f_{T_B} vs f_d).

structure should be taken into account. Furthermore, ejection of new components, possibly associated with $\gamma-$ray flares, may alter the innermost structure of the source, and a more methodic study, beyond the scope of this work, should be adopted (see e.g. Rioja et al. 2014). Additionally, given its dependence on the flux, it will not be straightforward to find a common factor for f_{T_B} either.

4.2. Extrapolation to Other Frequencies

Regarding the core size, it seems that the factor $f_d = 0.09$ considered here seems to be in agreement with the value expected considering the array resolution, once we consider the actual baselines and UV coverage during the observations. It is thus reasonable to consider that, at different frequencies, this factor will be scaled accordingly. On the other hand, given the characteristics for f_S and hence f_{T_B}, considerations for the brightness temperature may not be straightforward.

In Lee (2014), it is discussed that, in general for AGNs, $T_b \propto \nu^{\xi}$, with $\xi = +2.6$ below a critical frequency ν_c, which corresponds to the peak frequency of the spectrum. Beyond this frequency, $\xi \sim -1$ for a decelerating jet model and $\xi \sim +1$ for the rapidly accelerating jet model. In that work, it was found that the brightness temperature seemed to decrease with frequency as $T_b \propto \nu^{-1.2}$ for $\nu > 9$ GHz, favoring the decelerating jet model. However, in Lee et al. (2016), the median brightness temperatures increase from $T_b = 10^9\ K$ at 22 GHz to $T_b = 7.4 \times 10^9\ K$ at 129 GHz; i.e, increasing by almost an order of magnitude. Furthermore, the observed frequency dependence in Lee (2014) was significantly different than the predictions. These apparent inconsistencies could be potentially due to the blending effects discussed here. Only once these are understood, the physical model can be truly tested.

From our result above, we can consider that, statistically speaking, the actual brightness temperature at 43 GHz may be a factor ~ 50 larger than the one observed with KVN. If we assume an accelerating jet, it may be possible for the blending effects to be similar or larger at higher frequencies. However, under the assumption of a constant speed or decelerating jet, blending effects on the KVN should decrease at higher frequencies.

5. CONCLUSIONS

We investigate the effects of core blending effects on AGNs under the KVN view by comparing the properties of a sample of 25 sources when observed with the KVN and VLBA arrays. For this purpose, we collected data at 43 GHz from the KVN iMOGABA program and the 43 GHz BU-VLBA-Blazar program and supplemented it with some additional observations. Although the two data sets are not fully coincident in time, we consider various cases where quasi-simultaneous observations exist and study their effects on the discussed quantitites.

Our results suggest that, on average, the core flux densities are larger by a factor $f_S = 0.6$; the core sizes are larger by a factor $f_d = 0.09$, and the brightness temperatures are lower by a factor $f_{T_b} = 59$, when observed with the KVN. These factors are compatible with the a priori expectations purely based on the arrays different resolutions. Note however that, although a common blending factor f_d would suffice to characterize the KVN with respect to other VLBI arrays, there is a significant scatter in the fractional values for the flux density f_S and the brightness temperature $f_{T_b} = 59$. Such scatter may be attributed to the particular properties of each source, as suggested by previous results by Rioja et al. (2014).

We thus suggest that a factor $f_d = 0.09$ could be used to scrutinize KVN core size blending effects when comparing the VLBA and KVN at 43GHz. Otherwise, a source–dependent factor can also be estimated. We discuss considerations regarding the AGN jet model and possible implications of the relative magnitude of the blending effect at different frequency bands. Further work, including simulations and matching spatial resolutions of the observations will be the topic of future research.

ACKNOWLEDGMENTS

We are grateful to all staff members in KVN who helped to operate the array and to correlate the data. The KVN is a facility operated by the Korea Astronomy and Space Science Institute. The KVN operations are supported by KREONET (Korea Research Environment Open NETwork) which is managed and operated by KISTI (Korea Institute of Science and Technology Information). We acknowledge financial support from the Korean National Research Foundation (NRF) via Global Ph.D. Fellowship Grant 2014H1A2A1018695 and Basic Research Grant NRF-2015R1D1A1A01056807. S. S. Lee was supported by the National Research Foundation of Korea (NRF) grant funded by the Korea government (MSIP) (NRF-2016R1C1B2006697). J. W. Lee is grateful for the support of the National Research Council of Science and Technology, Korea (Project Number EU-16-001). This study makes use of 43 GHz VLBA data from the VLBA-BU Blazar Monitoring Program (VLBA-BU-BLAZAR; http://www.bu.edu/blazars/VLBAproject.html), funded by NASA through the Fermi Guest Investigator Program. The VLBA is an instrument of the National Radio Astronomy Observatory. The National Radio Astronomy Observatory is a facility of the National Science Foundation operated by Associated Universities, Inc.

REFERENCES

Algaba, J.-C., Zhao, G-Y., Lee, S. S., et al. 2015, Interferometric Monitoring of Gamma-Ray Bright Active Galactic Nuclei II: Frequency Phase Transfer, JKAS, 48, 237

Algaba, J.-C., Lee, S. S., Kim, D. W., et al. 2018, Exploring the Variability of the Flat Spectrum Radio Source 1633+382. I. Phenomenology of the Light Curves, ApJ, 852, 30

Algaba, J.-C., Lee, S. S., Rani, B., et al. 2018, Exploring the Variability of the Flat-spectrum Radio Source 1633+382. II. Physical Properties, ApJ, 859, 128

Asada, K., Nakamura, M., & Pu, H. Y. 2016, Indication of the Black Hole Powered Jet in M87 by VSOP Observations, ApJ, 833, 56

Boccardi, B., Krichbaum, T. P., Bach, U., et al. 2016, First 3 mm-VLBI Imaging of the Two-sided Jet in Cygnus A. Zooming into the Launching Region, A&A, 588, 9

Bruni, G., Gómez, J. L., Casadio, C., et al. 2017, Probing the Innermost Regions of AGN Jets and Their Magnetic Fields with RadioAstron. II. Observations of 3C 273 at Minimum Activity, A&A, 604, 111

Hada, K., Kino, M., Doi, A., et al. 2013, The Innermost Collimation Structure of the M87 Jet Down to ∼10 Schwarzschild Radii, ApJ, 775, 70

Hodgson, J., Lee, S. S., Zhao, G.-Y., et al. 2016, The Automatic Calibration of Korean VLBI Network Data, JKAS, 49, 137

Gómez, J. L., Lobanov, A. P., Bruni, G., et al. 2016, Probing the Innermost Regions of AGN Jets and Their Magnetic Fields with RadioAstron. I. Imaging BL Lacertae at 21 Microarcsecond Resolution, ApJ, 817, 96

Hovatta, T., Valtaoja, E., Tornikoski, M., et al. 2009, Doppler Factors, Lorentz Factors and Viewing Angles for Quasars, BL Lacertae Objects and Radio Galaxies, A&A, 494, 527

Hovatta, T., Lister, M. L., Aller M. F., et al. 2012 MOJAVE: Monitoring of Jets in Active Galactic Nuclei with VLBA Experiments. VIII. Faraday Rotation in Parsec-scale AGN Jets, AJ, 144, 105

Hovatta T., Aller, M. F., & Aller, H. D. 2014, MOJAVE: Monitoring of Jets in Active Galactic Nuclei with VLBA Experiments. XI. Spectral Distributions, AJ, 147, 143

Jorstad, S. G., Marscher, A. P., Morozova, D.A., et al. 2017, Kinematics of Parsec-scale Jets of Gamma-Ray Blazars at 43 GHz within the VLBA-BU-BLAZAR Program, ApJ, 846, 98

Kang, S.-C., et al. 2019, in preparation

Kardashev, N. S., Alakoz, A. V., Andrianov, A. S., et al. 2017, RadioAstron Science Program Five Years after Launch: Main Science Results, Solar Syst. Res., 51, 535

Kim, D.-W., Trippe, S., Lee, S. S., et al. 2017, The Millimeter-Radio Emission of BL Lacertae During Two γ-ray Outbursts, JKAS, 50, 167

Kim, J.-Y., Lee, S. S., Hodgson, J. A., et al. 2018, Long-term Millimeter VLBI Monitoring of M 87 with KVN at Milliarcsecond Resolution: Nuclear Spectrum", A&A, 610, 5

Kim, J.-Y., et al. 2019, in preparation

Kovalev, Y. Y., Lobanov, A. P., Pushkarev, A. B., et al. 2008, Opacity in Compact Extragalactic Radio Sources and Its Effect on Astrophysical and Astrometric Studies, A&A, 483, 759

Lee, S. S., Han, M. H., Kang, S. C., et al. 2013, Monitoring of Multi-frequency Polarization of Gamma-ray Bright AGNs, Eur. Phys. J. Web Conf., 6107007L

Lee, S. S. 2014, Intrinsic Brightness Temperatures of Compact Radio Jets as a Function of Frequency, JKAS, 47, 303

Lee, S. S., Wajima, K., Algaba, J. C., et al. 2016, Interferometric Monitoring of Gamma-Ray Bright AGNs. I. The Results of Single-epoch Multifrequency Observations, ApJS, 227, 8

Lee, J. W., Lee, S. S., Hodgson, J. A., et al. 2017, Interferometric Monitoring of Gamma-Ray Bright AGNs: S5 0716+714, ApJ, 841, 119

Ly, C., Walker, R. C., & Junor, W. 2007, High-Frequency VLBI Imaging of the Jet Base of M87, ApJ, 660, 200

Mahmud, M., Coughlan, C. P., Murphy, E. et al. 2013, Connecting Magnetic Towers with Faraday Rotation Gradients in Active Galactic Nuclei Jets, MNRAS, 431, 695

Pilipenko, S. V., Kovalev, Y. Y., Andrianov, A. S., et al. 2018, The High Brightness Temperature of B0529+483 Revealed by RadioAstron and Implications for Interstellar Scattering", MNRAS, 474, 3523

Pushkarev, A. B., Hovatta, T., Kovalev Y. Y., et al. 2012, MOJAVE: Monitoring of Jets in Active Galactic Nuclei with VLBA Experiments. IX. Nuclear Opacity, A&A, 545, 113

Rioja, M., Dodson, R., Jung, T. H., et al. 2014, Verification of the Astrometric Performance of the Korean VLBI Network, Using Comparative SFPR Studies with the VLBA at 14/7 mm, AJ, 148, 84

Wagner, S. J. & Witzel, A. 1995, Intraday Variability In Quasars and BL Lac Objects, ARA&A, 33, 163

Walker, R. C., Hardee, P. E., Davies, F. B., et al. 2018, The Structure and Dynamics of the Subparsec Jet in M87 Based on 50 VLBA Observations over 17 Years at 43 GHz, ApJ, 855, 128